Comparison of Multi-Sensor Admittance Control in Joint Space and Task Space for a Seven Degree of Freedom Upper Limb Exoskeleton

Levi Makaio Miller *,** and Jacob Rosen**
Dept. of Mechanical Engineering, University of Washington, Seattle WA*
Dept. of Computer Engineering, University of California Santa Cruz, Santa Cruz, CA**
E-mails: makaio@uw.edu, rosen@ucsc.edu, Bionics Lab URL: http://bionics.soe.ucsc.edu

Abstract—Control and overall system performance of an upper limb exoskeleton, as a wearable robot, is dictated in part by the human machine interface and the implemented control algorithm. The ultimate goal is to develop algorithms so the operator feels as if the exoskeleton is a natural extension the body. The aim of the current research is to compare the system performance of a 7 degree of freedom wearable upper limb exoskeleton (EXO-UL7) using two multi-sensor admittance controllers (1) task space control and (2) joint space control. Multiple force sensors are needed due to the redundancy in the system (7 DOF). This redundancy is explored and a method is developed to calculate a closed form inverse kinematics (IK) solution. The IK solution is used to develop the task space controller. The joint space controller uses the transpose of the jacobian to resolve sensor forces into joint torques. Six subjects performed a peg in hole task. Six targets covered the main part of the device workspace. Velocities and Interaction forces at the upper arm, lower arm, handle and tip were recorded during the experiments. Power exchange between the subject and device was calculated. Task space based control was about 11% lower in mean interaction energy for the peg in hole task compared to joint space control. Task completion time increased with both controllers compared to back-driving the device.

I. INTRODUCTION

Integrating capabilities of humans and robotic-machines into a unified system offers numerous opportunities for developing a new generation of assistive technology. For many physical tasks, human performance is limited by muscle strength. Similarly, muscle weakness is the primary cause of disability for persons with a variety of neuromuscular diseases including stroke, spinal cord injury, muscular dystrophies, and other neuro-degenerative disorders. Opposite this limitation in muscular strength, humans possess specialized and complex algorithms for control of movement, involving both higher and lower neural centers. These algorithms enable humans to perform very complicated tasks such as locomotion and arm movement, while at the same time avoiding object collisions. In contrast, robotic manipulators can be designed to perform tasks requiring large forces or moments, depending on their structure and on the power of their actuators. However, the control algorithms that govern their dynamics lack the flexibility to perform in a wide range of conditions while preserving the same quality of performance as humans. It seems therefore that combining these two entities, the human and the robot, into one integrated system under the control of the human, may lead to a solution which will benefit from the advantages of each subsystem. At the heart of this human-machine integration lie two fundamental scientific and technological issues: (i) the exoskeleton (orthotic device) mechanism itself and its biomechanical integration with the human body, and (ii) the human machine interface (HMI). These two key issues will determine the quality of the integration between the human and the exoskeleton.

Throughout the last three decades, several designs of exoskeletons for human power amplification have been developed and evaluated. In studying the evolution of these systems, two basic types with different Human Machine Interfaces (HMI) seem to emerge, which may be defined as generations. The first exoskeleton generation was developed based on the mission profile of the US Department of Defense that defined the exoskeleton as a powered suit to augment the lifting and carrying capabilities of soldiers. It was originally named man-amplifier. The primary intent was to develop a system that would greatly increase the strength of a human operator while maintaining human control of the manipulator. The first generation prototype, known as Hardiman, was the first attempt to mechanically design a man-amplifying exoskeleton using a hydraulically powered articulating frame worn by an operator [19], [5], [6], [17]. The position-controlled architecture led to poor responsiveness and instability. The second generation of exoskeletons placed the HMI at the dynamics level, utilizing the direct contact forces (measured by force sensors) between the human and the machine as the main command signals to the exoskeleton. The human wore the extender, in a way that linked them together mechanically. The operator was in full physical contact with the exoskeleton throughout its manipulation [30][13][14][11][12] [10][24]. Several experimental extender prototypes were designed and built in order to study issues associated with this mode of control.

This paper develops two different admittance controllers for a seven degree of freedom (DOF) exoskeleton. The first controller uses the force interactions between the device and the user to create trajectories directly in task space. The second, resolves the interaction forces into joint torque equivalents before creating trajectories in joint space. The performance of the two are compared while preforming a peg in hole task.

II. METHOD

A. Human Arm Model

The upper limb is composed of segments linked by articulations with multiple degrees of freedom. It is a complex structure that is made up of both rigid bone and soft tissue. Although much of the complexity of the soft tissue is difficult to model, the overall arm movement can be represented by a much simpler model composed of rigid links connected by joints. Three rigid segments, consisting of the upper arm, lower arm and hand, connected by frictionless joints, make up the simplified model of the human arm. The upper arm and torso are rigidly attached by a ball and socket joint. This joint is responsible for shoulder abduction-adduction (abd-add), shoulder flexion-extension (flx-ext) and shoulder internal-external (int-ext) rotation. The upper and lower arm segments are attached by a single rotational joint at the elbow, creating elbow flx-ext. Finally, the lower arm and hand are connected by a three axis spherical joint resulting in pronation-supination (pron-sup), wrist flx-ext, and wrist radial-ulnar (rad-uln) deviation.

Korein [15] was one of the first to study this seven DOF model. Since then, many other researches have used it to study movement for computer graphics [9] [16], redundant robots [8], upper limb exoskeletons [20] [21] [22] [26], biomechanics [27] [29] [28], and much more. This model does neglects motion of the scapula and clavicle, for this reason, others have used five [7] or even seven DOF [18] models of the shoulder, the 7 DOF model gives a good combination of motion accuracy while reducing the model complexity. This model of the arm is a redundant model.
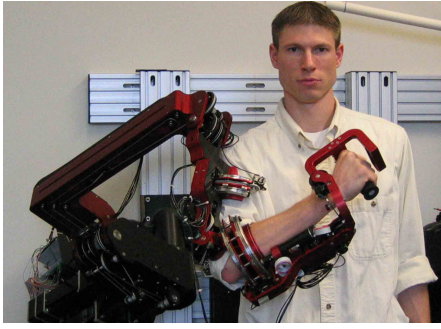
Fig. 1. The seven degree of freedom exoskeleton supports 99% of the ranges of motion required to preform daily activities
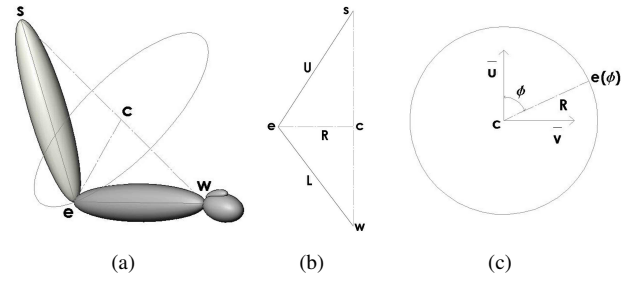

Fig. 2. a) The extra degree of freedom of the arm is defined by a rotation axis that goes from the shoulder to the wrist. b) The shoulder, elbow and wrist form the triangle sew. c) By creating a coordinate frame at the center of the elbow circle the swivel angel can be defined allowing the parameterizations of the elbow position by a single variable

B. Exoskeleton Design

The kinematics and dynamics of the human arm during activities of daily living (ADL) were studied in part to determine the engineering specifications for the exoskeleton design [Fig. 1] [20] [21]. Articulation of the exoskeleton is achieved about seven single axis revolute joints. The range of motion of the exoskeleton support 99% of the ranges of motion required to perform daily activities [21]. A result of representing the ball and socket joint of the shoulder as three intersecting joints, is the introduction of singularities not present in the human arm. A significant consideration in exoskeleton design is placement of singularities [22]. For the exoskeleton arm, singularities occur when joints 1 and 3, or joints 3 and 5 align. To minimize the frequency of this occurrence, the axis of joint 1 is positioned such that singularities with joint 3 takes place only at locations that are anthropometrically hard to reach. With each of these singularity vectors at or near the edge of the human workspace, the middle and majority of the workspace is free of singularities [20] [21].

The human machine interface (HMI) consists of three attachment point on the exoskeleton. One attachment point is for the upper arm, one is for the lower arm, and the last is for the hand. The hand HMI consists of a handle, the upper and lower arm HMIs consists of a pressure distributive structural pad that securely straps to the mid-distal portion of each respective arm segment. Each interface is rigidly attached to a 6-axis force/torque sensor (ATI Industrial Automation, model - Mini 40) that is in turn rigidly attached to the exoskeleton. These sensors allow every force and torque interactions between the exoskeleton and the user to be measured. A forth force/torques sensor at the tip of the exoskeleton allows measurement interactions between the exoskeleton and the environment.

C. The Extra Degree of Freedom

The seven DOF arm model is redundant. Knowing the location of the hand does not fully specify the configuration of the arm. The exoskeleton supports the entire arm, so the configuration is important. By also specifying the elbow position, the arm configuration is fully defined. The elbow position introduces three additional variables where only one additional variable is needed. A single variable can parameterize the elbow. The arm forms a triangle with a point at the shoulder (s) one at that the elbow (e) and the last at the wrist (w). Both the shoulder and wrist joint are spherical, and allow rotation of point e around the vector $(w - s)$ [Fig. 2(a)].

A local coordinate system at the center of the elbow circle (c), gives a reference to measure the swivel angle (ϕ) of the elbow. Create a normal vector that points in the same direction as $(w - s)$.

$$\vec{n} = \frac{w - s}{||w - s||} \qquad (1)$$

Next project and normalize a vector onto the plane normal to $\vec{n}$.

$$\vec{u} = \frac{\vec{a} - (\vec{a} \cdot \vec{n})\vec{n}}{||\vec{a} - (\vec{a} \cdot \vec{n})\vec{n}||} \qquad (2)$$

where $\vec{a}$ can be selected as any vector. Badler and Torlani [1] suggest $\vec{a}$ to be the $-\vec{z}$ vector. This selection has real physical meaning. When ϕ is equal to zero, the elbow is at its lowest possible point. A mathematical singularity occurs whenever the vectors $\vec{n}$ and $\vec{a}$ are parallel. If $\vec{a}$ is chosen to be equal to $-\vec{z}$, then every time the arm is at the side, in a rest position, equation (2) will be at or near a singularity. So we will place the mathematical singularity of equation (2) in the same location as the exoskeleton's singularity. This is achieved by selecting $\vec{a}$ to point in the direction of the rotation axis of joint 1. The last vector of the coordinate system ($\vec{v}$), is found taking by the cross product of $\vec{n}$ and $\vec{u}$. Vectors $\vec{n}$, $\vec{u}$ and $\vec{v}$ form an orthonormal coordinate system. Where $\vec{u}$ and $\vec{v}$ are in the plane of the elbow circle [Fig. 2(c)]. The radius (R) and center (c) of the circle are easily found through geometry.

$$R = U \sin(\alpha) \qquad (3)$$
$$c = s + U \cos(\alpha) \cdot \vec{n} \qquad (4)$$
$$\cos(\alpha) = \frac{U^2 - L^2 - ||w - s||^2}{-2L^2 ||w - s||} \qquad (5)$$

Where U and L are the length of the upper and lower arm segments [Fig. 2(b)]. Now the position of the elbow can now be expresses as a parametrization of ϕ [25].

$$e(\phi) = R \left[\cos(\phi)\vec{u} + \sin(\phi)\vec{v} \right] + c \qquad (6)$$

D. Inverse Kinematics

There are several methods to do inverse kinematics on redundant manipulators [3], [4]. Many of then use the pseudoinverse of the jacobian where the null space is used to achieve secondary objectives [2]. In our case we are going to specify the swivel angle, and thus making the problem no longer redundant. The inverse kinematic problem now consists of solving for all the joint angles such that the two following problems are satisfied.

$$T_1 T_2 T_3 T_4 T_5 T_6 T_7 g_{st} = g_d \qquad (7)$$
$$T_1 T_2 e_0 = e(\phi) \qquad (8)$$

Where T_i is the 4×4 transformations matrix from the link frame $i - 1$ to link frame i. g_{st} is the transformation matrix from the 7th link frame to the end effector frame. g_d is the transformation matrix that represents the desired end effector position and orientation. e_o is the initial position of the elbow, and $e(\phi)$ is from equation (6). It is fairly straight forward to solve for the joint angels from this system of equations.

E. Admittance control

Typically, in admittance control a force sensor is attached to the end effector of a robot, then the input from this sensor is used to produce velocity commands for the device. The redundancy in our device creates problems with this model, not only do we have to specify the velocity of the handle, velocities for the elbow angle must also be specified. Several algorithms have been developed to select the elbow angle, including creating selection criteria based on kinematic, dynamic and biomechanical data [16]. Creating heuristics based on observations of movement [27], and several iterative methods used to avoid obstacles and joint limits [9], or that use dynamic information [28]. Although these algorithms can create natural reach motions, the exoskeleton device needs to track the motion of the user in all situation. The above mentioned algorithms lack the flexibility of real time use where even small differences in the exoskeleton position, and the users desired position, can cause discomfort. For this reason additional force sensors track the interactions of the user and the device at the upper arm and lower arm.

There are two fundamental way that the admittance control can be implemented. The first is to compute a trajectory in task space then use inverse kinematics to calculate the joint angles. The second is to transform the force/torques signals into joint torque equivalents, then create joint trajectories directly from the torque signals.

F. Task Space Admittance Control

In task space admittance control, the hand position, orientation and the elbow angle are calculated independently in task space using the four force sensors. Then the trajectory of the hand as well as the swivel angle are put through the inverse kinematic function. The joint trajectories are followed using PID control.

1) Wrist Position: The position of the wrist is influenced by the force interactions from each of the four forces sensors. It is straight forward to relate the forces at the tip ($\vec{f_t}$), handle ($\vec{f_h}$) and lower arm ($\vec{f_l}$), to changes in position at the wrist. Each of these locations have three DOF of translational motion. They each span all of R^3 and the device will not constrain the translational motion at any of these locations. The motions of the device due to the interaction forces will be in the same direction as the force vector. It is not as straight froward for the upper arm, where there are only two translational degrees of freedom. The spherical joint of the shoulder constrains any point on the upper arm to the surface of a sphere. A force applied on the upper arm that is tangent to this sphere, can move it along the surface. If the force is applied perpendicular to the sphere, the device resists the force and no motion occurs. A spherical trajectory of the upper arm creates spherical trajectory at the wrist. However, the motion at the wrist is not always in the same direction as the force vector at the upper arm.

To relate the direction of the upper arm forces and the motion at the wrist, define a frame at the origin of the upper arm force sensor. Let x point to the users right, y point forward and z point up when the arm is at the side. The z component of the upper arm force signal is always perpendicular to the sphere of motion, so the z component of the the signal is set to zero. The x component of the signal creates motion at the wrist in the same direction as the upper arm, because the x vector is tangent to the sphere of motion of both the upper arm and wrist [Fig. 3(a)]. When the elbow is bent, the vectors tangent to the surface of the spheres at the wrist and upper arm are separated by the angle α, previously defined in equation (5). Because motion must be tangent to these vectors, a motion in the y direction at the sensor, will cause a motion at the wrist that is rotated by an angle α [Fig. 3(b)]. Taking these considerations into mind, the original upper
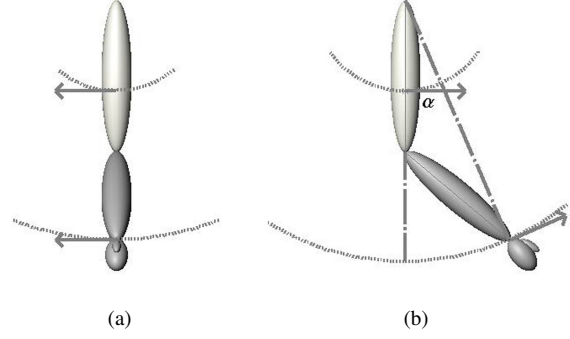

Fig. 3. Force interactions at the upper arm create motion that is tangent to a sphere that is centered at the shoulder. a) The x component of an upper arm force creates motion in the x direction at the upper arm and wrist. b) The y component of the force creates a motion in the y direction at upper arm but the motion is rotated by α at the wrist. The z component is resisted by the mechanism and does not result in motion

force signal ($\vec{f_u}$) gets transformed as follows:

$$\vec{f_u} = \begin{bmatrix} x \\ y \\ z \end{bmatrix} \Rightarrow \begin{bmatrix} x \\ y \\ 0 \end{bmatrix} \Rightarrow \begin{bmatrix} x \\ cos(\alpha)y \\ sin(\alpha)y \end{bmatrix} \tag{9}$$

To work with the four sets of forces signals, they must all be in a common frame.

$$\vec{f'} = R_1 R_2 \dots R_n \vec{f} \tag{10}$$

where $\vec{f}$ is the force measurement, n is the link frame that the sensor is attached to, and $\vec{f'}$ is the force represented in the global frame. If the arm and exoskeleton device are moving together perfectly, the force between the user and the device should be zero. Therefore we will use zero as our reference force, and the error in the force ($\vec{f_e}$) will be.

$$\vec{f_e} = \vec{f_u}' + \vec{f_l}' + \vec{f_h}' + \vec{f_t}' - \vec{0} \tag{11}$$

In this model the forces are all weighted evenly. Next, transform the force signals into a task space position signal.

$$x = k_p \vec{f_e} + k_i \int \vec{f_e} - k_d \dot{x} \tag{12}$$

The last term ($-k\dot{x}$) is not directly related to the force error, because force sensors have a lot of noise, taking the derivative can be a problem. If force is approximated with hooks law

$$F = -K(x - x_0) \quad \Rightarrow \quad \dot{F} = -K\dot{x} \tag{13}$$

we can get an approximate derivative of the force without having to deal with a noisy force signal [23].

2) Wrist Orientation: Changes in the wrist orientation are calculated based on torque at the wrist. The upper and lower force sensors produce no torque on the wrist. The handle and tip force sensor will produce torques at the wrist. Neither the wrist or the tip sensors are located at the wrist. Therefore the torque at the wrist ($\vec{\tau_w}$) due to the handle, will be the addition of the handle torque ($\vec{\tau_h}$) with the cross product of the handle distance ($\vec{r_h}$) and the handle force ($\vec{f_h}$). Similarly, The torque at the wrist due to the tip will be the tip torque ($\vec{\tau_t}$) plus the cross product of the tip distance ($\vec{r_t}$) with the tip force ($\vec{f_t}$). The total torque at the wrist will be the addition of the contributions of the handle and the tip. Next transform $\vec{\tau_w}$ from the sensor frame into the global frame.

$$\vec{\tau_w} = \left[\vec{\tau_h} + (\vec{r_h} \times \vec{f_h})\right] + \left[\vec{\tau_t} + (\vec{r_t} \times \vec{f_t})\right] \tag{14}$$

$$\vec{\tau_w}' = R_1 R_2 R_3 R_4 R_5 R_6 R_7 \vec{\tau_w} \tag{15}$$

The desired reference torque is zero, making the error signal

$$\vec{\tau_e} = \vec{\tau_w}' - \vec{0} \tag{16}$$

Taking $\vec{\tau_e}$ to be the axis angle representation for the change in orientation, a rotation matrix (R_e) can be constructed to represent the desired change.

$$\theta_e = ||\vec{\tau_e}|| \tag{17}$$
$$\vec{\omega_e} = \frac{\vec{\tau_e}}{\theta_e} \tag{18}$$
$$R_e = I + \hat{\omega}_e \, \sin(\theta_e) + \hat{\omega}_e{}^2(1 - \cos(\theta_e)) \tag{19}$$

Where θ_e is the desired change in angle, $\vec{\omega_e}$ is the rotation axis, I is the 3×3 identity matrix, and $\hat{\omega}_e$ is the antisymmetric matrix equivalent of the cross product. With this, the desired orientation (R_d) is then:

$$R_d \quad = \quad R_e R_{d-1} \tag{20}$$

Where R_{d-1} is the desired orientation from the previous time step. At initiation R_{d-1} is set equal to the current orientation of link 7.

3) Swivel Angle: Changes in the swivel angle are calculated based on the torque on the swivel axis. The handle and tip forces are not used for this calculation. The upper and lower arm forces both contribute to the torque around the swivel axis. The upper and lower arm sensors are measured in different frames and have to be put into the common global frame. The sensors are not located on the rotation axis, so the applied torque on the axis must be calculated. The torque on the shoulder as a result of the upper sensor is equal to the torque at the upper sensor ($\vec{\tau_u}'$) added to the cross product of the vector from the shoulder to the upper sensor ($\vec{r_u}$) with the upper force ($\vec{f_u}'$). Similarly, the torque on the shoulder, as a result of the lower forces, is equal to the torque at the lower arm ($\vec{\tau_l}'$) plus the cross product of the vector from the shoulder to the lower sensor ($\vec{r_l}$) with the lower force ($\vec{f_l}'$). The total torque on the shoulder ($\vec{\tau_s}$) is the addition of the contributions from the upper and lower arm.

$$\vec{\tau_s} = \left[\vec{\tau_u}' + (\vec{r_u} \times \vec{f_u}') \right] + \left[\vec{\tau_l}' + (\vec{r_l} \times \vec{f_l}') \right] \tag{21}$$

Only the component of torque that acts on the swivel axis will cause a change in the swivel angle. The component of $\vec{\tau_s}$ acting on $\vec{n}$ (from Eqn. (1)) is fould by taking the dot product of the two.

$$\vec{\tau_n} \quad = \quad \vec{\tau_s} \cdot \vec{n} \tag{22}$$

The desired reference torque is zero so the error is equal to $\vec{\tau_e} = \vec{\tau_n} - 0$ and the desired swivel angle is:

$$\phi \quad = \quad k_p \, \vec{\tau_e} + k_i \int \vec{\tau_e} - k_d \, \dot{\phi} \tag{23}$$

Like equation (12) the term ($-k_d \, \dot{\phi}$) is an approximation of the derivative of the torque.

Equations (12), (20) and (23) define the desired position, orientation and swivel angle for a given time step. The desired joint angles are then calculated using the inverse kinematics. A PID position controller moves the exoskeleton to the desired joint angles.

G. Joint Space Admittance Control

In joint space control, the forces and torques from the four sensors are first transformed into the joint torque equivalents. Then changes in joint position are calculated. The transformation is achieved by multiplying the force/torque signal ($F = [\vec{f}, \vec{\tau}]^T$) by the jacobian transpose (J^T).

$$\Gamma = J^T F \tag{24}$$

The jacobian from the base to each of the force sensors have to be calculated. The upper sensor jacobian (J_u) will be a 6×3 matrix. The lower sensor jacobian (J_l) will be a 6×5 matrix. The handle sensor jacobian (J_h) will be a 6×7 matrix, and the tip sensor jacobian (J_t) will be a 6×7 matrix. The total joint torque on each joint is the summation of the individual joint torques that result from each sensor location. The upper and lower sensors, however do not contribute to joint torques of joints located distally. In order to add the vector quantities, append zeros to Γ_u and Γ_l till they are both 7×1 vectors. With all the vectors the same dimension, they can be added.

$$\Gamma_j = \Gamma_u + \Gamma_l + \Gamma_h + \Gamma_t \tag{25}$$

Finally the desired joint position has to be calculated. The desired reference force for all the sensors is zero. With this, the torque error (Γ_e) is equal to Γ_j and the desired joint position becomes

$$\theta_j = k_p \Gamma_e + k_i \int \Gamma_e - k_d \dot{\theta}_j \tag{26}$$

H. Experimental Setup

This experiment compares movement of the device with task space admittance control using four sensors as described in section II-F and movement of the device with joint space movement control using four sensors as described in section II-G. Additionally the motion of manual control (back-driven with no control effort) were recorded.

The height, age and sex of each subject was taken at the beginning of each experiment. The exoskeleton's height was adjusted for each user in a seated position. The subject was secured in the device by two straps, one at the upper arm and the other at the lower arm, additionally the user held a handle. In front of the subject was a table with 3 plastic targets, each with two slotted holes that matched a slotted peg on the tip of the device. The targets are numbered 1 to 6 from the subjects top right to bottom left. The location of the targets were, target 1 - [.450,.431,.870], target 2 - [.450,.431,.978], target 3 - [.09,.597,.870], target 4 - [.09,.597,.978], target 5 - [-.325,.575,.870], target 6 - [-.325,.575,.978], with x being to the subjects right, y being in front of the subject and z pointing up. x and y are measured from the center of the shoulder, z is measured from the floor, all units are in meters [Fig. 4]. In the users left hand was an enable button which released the brakes on the device and engaged the motors. Each subject was instructed to begin with their arm at their side, with the enable button disengaged. The experimenter would then tell them a target to move to, they then press the enable button, insert the peg into the hole, return their arm to the side, and release the enable button. For each experiment there were 6 targets. Each control scheme moved to each target once in random order. Four repetitions were repeated for each subject, and each subject was asked if they needed a break between repetitions.

Six subjects participated in the experiment. There was a mix of male and female subjects with a range of ages and heights, see table I. Subject 4 was unable to complete the tasks under manual control. A total of 395 trails were recorded consisting of, 118 trials for manual control, 134 trials for joint space control and 143 trials for task space control. Statistical significants was determined using Matlab's anovan and multcompare functions. The 95% confidence level was selected as significant for this study.

III. RESULTS

1) Power: The linear and angular power exchange at each sensor was calculated by multiplying the recorded force/torque by its respective velocity. The velocities we calculated at each sensor by differentiating the position of each sensor. Figure 5 shows the average power exchange for manual control, joint space control and task space control after they have been normalized with respect to time.

Subject	Sex	Age	Height (m)	Exoskeleton Height (m)
1	m	21	1.74	0.86
2	m	23	1.88	0.89
3	m	43	1.74	0.86
4	f	25	1.63	0.79
5	m	22	1.73	0.82
6	f	21	1.70	0.82

Fig. 4. A subject inserts the tip of the exoskeleton into a target. There was a total of 6 targets. Each subject performed 4 repetitions of every controller moving to every target

2) Energy: The energy exchange between the exoskeleton and subject was calculated for each trial by integrating the power. Additionally the negative and positive components of the energy were each computed separately. Figure 6 shows the distribution of energy for the over all energy (Fig. 6(a)), the negative energy component (Fig. 6(b)), and the positive energy component (Fig. 6(c)). Table II reports the minimum, 25th percentile, median, 75th percentile, maximum and mean with its 95% confidence interval for each of the box plots in figure 6.

The differences in mean for the overall energy was statistically significant for all three groups. For the negative component, manual control was statically different from joint and task space control. Joint and task space control were not statistically different from each other. For positive energy component, joint space control was statistically different from manual and task space control. Manual and task space control were not statistically different from one another.

3) Completion time: The completion time for each trial was calculated from when the subject first pressed the enable button at the beginning of the movement to when they released it at the end of the movement. Figure 6(d) shows the distribution of completion times for manual control, joint space control and task space control. Table
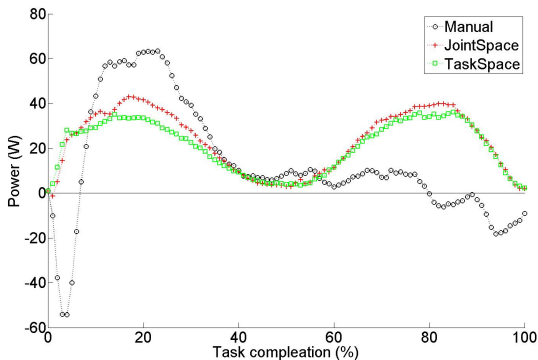

Fig. 5. Power normalized with respect to time then averaged over all reach tasks for manual control, joint space control and task space control.

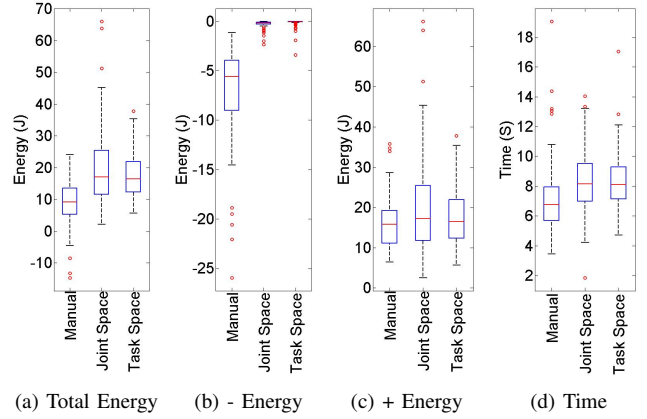(a) Total Energy (b) - Energy (c) + Energy (d) Time

Fig. 6. Distribution of interaction energy and completion time. a) Total energy interaction b) negative energy interaction c) Positive energy interaction d) Completion time

TABLE II

| | | 1st | | 3ed | | |
	Min	Quartile	Median	Quartile	Max	Mean
Total Energy (J)						
Manual	-14.70	5.29	9.19	13.52	24.16	9.29 ($\pm$ 1.11)
Joint Space	2.13	11.61	17.06	25.44	66.04	19.55 $\pm$ 1.04
Task Space	5.69	12.31	16.44	21.96	37.77	17.43 $\pm$ 1.01
Negative Energy (J)						
Manual	-25.97	-9.00	-5.58	-3.93	-1.14	-6.92 $\pm$ 0.34
Joint Space	-2.34	-0.28	-0.17	-0.083	-0.007	-0.25 $\pm$ 0.34
Task Space	-3.41	-0.054	-0.028	-0.013	-0.00067	-0.098 $\pm$ .33
Positive Energy (J)						
Manual	6.41	11.12	15.84	19.23	35.77	16.21 $\pm$ 1.10
Joint Space	2.50	11.77	17.27	25.49	66.21	19.81 $\pm$ 1.03
Task Space	5.71	12.35	16.45	21.97	37.83	17.52 $\pm$ .99
Completion Time (sec)						
Manual	3.45	5.69	6.75	7.94	19.06	7.03s $\pm$ .28s
Joint Space	1.84	6.98	8.15	9.51	14.04	8.14 $\pm$ .26s
Task Space	4.71	7.16	8.11	9.30	17.03 s	8.34 $\pm$ .25s

II reports the minimum, 25th percentile, median, 75th percentile, maximum and mean with its 95% confidence interval for the box plot in figure 6(d). Manual control was statistically different from joint and task space control.

IV. DISCUSSION

Figure 5 shows the average power exchange between the subject and exoskeleton during reach tasks. It should be noted that this power is only the exchange of power between the two systems and does not say anything about the total power used by either system. In this figure it is easy to identify three distinct regions of motion. From 0% to about 40% of task completion the subject is raising the arm from their side up to the level of the target. From about 40% to 60%, the target is being engaged, and from about 60% to 100% the arm is being lowered back down to the side of the body. In region one we see that manual control has a sharp drop with a negative power peaking about -58W, followed by a steep increase to a positive power of around 65W and finally has a decline to around 10W. The sharp decrease is due to to the device falling slightly after the breaks are disengaged. The arm is then accelerated up wards to the level of the target increasing the power, finally the acceleration is decreased as the target is approached. Joint and task space control have a similar rise and fall on the power curve but without the initial drop as the controllers prevented the exoskeleton from falling when the breaks are released. In region 2, the subjects are engaging the targets. for all three control types the power was low, between 5 and 10 watts. In this region the motion was much slower as the peg is inserted into the hole. Additionally the motion was in the transverse plane

so gravitational forces were not in the direction of motion, making the power much lower for this region. The third region is the most interesting. For manual control, power is low and positive for about half the region and low and negative for the other half. As the subject lowers the arm, gravity pulls it in the same direction as the motion creating a very low power. The plots would indicate that initially the subject was moving slightly faster then gravity was pulling the arm down, then at about 80% of task completion, the subject began to slow the arm and gravity pulled the arm faster then they wanted to go. The two admittance controllers produce a power profile that is very similar to region one, where there is an increase to the power followed by a reduction to 0W. It would be easy to interpret this as meaning the admittance controllers made it harder to lower the arm, This would be an incorrect interpretation of the data. The power plot is power exchanged between the device and subject, not the power exerted by the subject. For an admittance controller the power exchange should always be positive, as the device should only move in the direction that you are pushing it. In fact having a similar power profile for region one and three shows uniform performance for both raising and lowering the arm.

The total energy for manual control is lowest for all the controllers. Because the admittance controllers have almost no negative power, we would expect them to have a higher energy then the manual control. It is more insightful to look at the negative and positive components of the energy and compare them separately. As expected the admittance controllers have almost no negative components and doesn't give us a lot of information to compare them. The positive energy component shows a statistically significant difference between the joint space and task space control. Task space control had about an 11.5% lower energy exchange then joint space control.

One surprising and undesirable result is that with manual control the completion time was shorter then with the controllers. The controllers should make the task easier so an equal or shorter time would be expected. This indicates that the bandwidth of the admittance controllers is lower then that of the human arm.

The admittance controllers both reduced the negative power to near zero indicating that the controllers were moving with the subject as desired. The task space controller had the best performance with a reduction to the average task energy of about 11.5%. This performance increase came at the cost of a more involved and harder to implement algorithm.

The task completion time suffered from the implementation of the controllers. Further work need to be done to address this problem. The gains of the controllers must be increased while still maintaining stability. One possibility might be to use a nonlinear gain, which will be higher during fast gross positioning motions and lower for slower precise motions. Alternatively motion prediction can be used reducing the delays in the system and allowing for faster motion. Currently we are exploring using the neural signals to predict the motion of the arm to increase the bandwidth and raise the gains.

V. ACKNOWLEDGMENTS

REFERENCES

[1] Norman I. Badler and Deepak Tolani. Real-time inverse kinematics of the human arm. *Presence*, 5(4):393–401, 1996.

[2] P. Baerlocher and R. Boulic. Task-priority formulation for the kinematic control of highly redundant articulated structures. In *IEEE/RJS Intl. Conference on Intelligent Robots and Systems*.

[3] Samuel R. Buss. Introduction to inverse kinematics with jacobian transpose, pseudoinverse and damped least squares methods. 2004.

[4] Samuel R. Buss and Jin-Su Kim. Selectively damped least squares for inverse kinematics. *Graphics, gpu, and game tools*, 10(3):37–49, 2005.

[5] General Electric Company. Exoskeleton prototype project, final report on phase I. Technical Report S-67-1011, Schenectady, New York, 1966.

[6] General Electric Company. Hardiman I prototype project, special interim study. Technical Report S-68-1060, Schenectady, New York, 1968.

[7] P. Culmer, A. Jackson, M.C. Levesley, J. Savage, R.Richardson, J.A. Cozens, and B.B Bhakta. An admittance control scheme for a robotic upper-limb stroke rehabilitation system. In *Engineering in Medicine and Biology 27th Annual Conference*, pages 5081–5084.

[8] Ioannis Iossifidis and Axel Steinhage. Controlling a redundant robot arm by means of a haptic sensor. In *ROBOTIK 2002, Leistungsstand - Anwendungen - Visionen*, pages 269–274, 2002.

[9] Marcelo Kallmann. Analytical inverse kinematics with body posture control. *Computer Animation and Virtual Worlds*, 2007.

[10] H. Kazerooni. The human amplifier technology at the university of california, berkeley. *Robotics and Autonomous Systems*, 19, 1996.

[11] H. Kazerooni and Ming-Guo Her. The dynamics and control of a haptic interface device. *Robotics and Automation*, 10(4), 1994.

[12] H. Kazerooni and Tanya J. Snyder. Case strudy on haptic devices: Human-induced instability in powered hand controllers. *Journal of Guidance, Control, and Dynamics*, 18(1):108–113, 1995.

[13] H. Kazerooni and R. Steger. The berkeley lower extremity exoskeleton. *Dynamic Systems, Measurements, and Control*, 128:14–25, 2006.

[14] H. Kazerooni, Ryan Steger, and Lihuna Huang. Hybrid control of the berkeley lower extremity exoskeleton (bleex). *The International Journal of Robotics Research*, (5-6):561–573, 2006.

[15] James U. Korein. *A Geometric Investigation of Reach*. MIT Press, 1985.

[16] Philip Lee, Susanna Wei, Jianmin Zhao, and Norman I. Badler. Strength guided motion. *Computer Graphics*, 24(4):253–262, 1990.

[17] B. J. Makinson. Research and development prototype for machine augmentation of human strength and endurance, hardiman I project. Technical Report S-71-1056, GE, Schenectady, New York, 1971.

[18] Walter Maurel. *3D Modeling of the Human Upper Limb Including the Biomechanics of Joints, Muscles amd Soft Tissues*. PhD thesis, Ecole Polytechnique Federale de Lausanne, 1998. These No 1906.

[19] R. S. Mosher. Force reflecting electrohydraulic servo manipulator. *Electro-Tech*, 138, 1960.

[20] Joel C. Perry and Jacob Rosen. Design of a 7 degree-of-freedom upper-limb powered exoskeleton. In *IEEE/RAS-EMBS International Conference on Biomedical Robotics and Biomechatronics*, 2006.

[21] Joel C. Perry, Jacob Rosen, and Stephen Burns. Upper-limb powered exoskeleton design. *Mechatronics*, 12(4):408–417, 2007.

[22] Jacob Rosen and Joel C. Perry. Upper limb powered exoskeleton. *International Jornal of Humanoid Robotics*, 4(3):529–548, 2007.

[23] Homayoun Seraji. Adaptive admittance control: An approach to explicit force control in compliant motion. In *Proceedings of the IEEE International Conference on Robotics and Automation*, pages 2705–2712, 1994.

[24] Tanya J. Snyder and H. Kazerooni. A novel material handling system. In *Proceedings of the 1996 IEEE International Conference on Robotics and Automation*, pages 1147–1152, 1996.

[25] Deepak Tolani, Ambarish Goswami, and Norman I. Badler. Ral-time inverse kinematics techniques for anthropomorphic limbs. *Graphucal Models*, 62:353–388, 2000.

[26] N.G. Tsagarakis and Darwin G. Caldwell. Development and control of a 'soft-actuated' exoskeleon for use in physiotherapy and training. *Autonomous Robots*, 15:21–33, 2003.

[27] Xuguang Wang. A behavior-based inverse kinematics algorithm to predict arm prehension posture for computer-aided ergonomic evaluation. *Journal of Biomechanics*, 32:453–460, 1999.

[28] Feng Yang and Xiugan Yuan. An inverse kinematical algorithm for human arm movement with comfort level taken into account. In *IEEE Conference on Control Applications*, volume 2, 2003.

[29] Xudong Zhang and Don B. Chaffin. The effects of speed variation on joint kinematics during multisegment reaching movements. *human movement science*, 18:741–757, 1999.

[30] Adam B Zoss, H. Kazerooni, and Andrew Chu. Biomechanical design of the berkeley lower extremity exoskeleton (bleex). *IEEE/ASME Transactions on Machatronics*, 11(2), 2006.